Reaction of nitric oxide molecules on transition-metal-doped silver cluster cations: size- and dopant-dependent reaction pathways

Arakawa, Masashi
Department of Chemistry, Faculty of Science, Kyushu University

Horioka, Masataka
Department of Chemistry, Faculty of Science, Kyushu University

Minamikawa, Kento
Department of Chemistry, Faculty of Science, Kyushu University

Kawano, Tomoki
Department of Chemistry, Faculty of Science, Kyushu University

他

出版情報：Physical Chemistry Chemical Physics. 23 (40), pp.22947-22956, 2021-09-22. Royal Society of Chemistry (RSC)
バージョン：
権利関係：

PAPER

Reaction of nitric oxide molecules on transition-metal-doped silver cluster cations: Size- and dopant-dependent reaction pathways†

Received 00th January 20xx,
Accepted 00th January 20xx

DOI: 10.1039/x0xx00000x

Masashi Arakawa,*[a] Masataka Horioka,[a] Kento Minamikawa,[a] Tomoki Kawano[a] and Akira Terasaki*[a]

We report size- and dopant-dependent reaction pathways as well as reactivity of gas-phase free Ag_nM^+ (M = Sc–Ni) clusters interacting with NO. Reactivity of Ag_nM^+, except for M = Cr and Mn, exhibits a minimum at a specific size, where the cluster cation possesses 18 or 20 valence electrons with 3d and 4s of the dopant as well as Ag 5s. The product ions range from NO adducts, $Ag_nM(NO)_m^+$, and oxygen adducts, $Ag_nMO_m^+$, to NO_2 adducts, $Ag_nM(NO_2)_m^+$. At small sizes, $Ag_nMO_m^+$ are the major products for M = Sc–V, whereas $Ag_nM(NO)_m^+$ dominate the products for M = Cr–Ni in striking contrast. In both cases, these reaction products are reminiscent of those from an atomic transition metal. However, the reaction pathways are different at least for M = Sc and Ti; kinetics measurements reveal that the present oxygen adducts are formed via NO adducts, while, for example, Ti^+ is known to produce TiO^+ directly by reaction with a single NO molecule. At larger sizes, on the other hand, $Ag_nM(NO_2)_m^+$ are dominantly produced regardless of the dopant element because the dopant atom is encapsulated by the Ag host; the NO_2 formation on the cluster is similar to that reported for undoped Ag_n^+.

1 Introduction

Nitric oxide (NO) is one of the toxic gases generated during combustion processes, e.g., in automobile engines and thermal power stations, causing environmental issues such as photochemical smog and acid rain. Catalytic reduction of NO is one of the important subjects in industrial chemistry. Since gas-phase reactions provide a fundamental framework of chemical and physical processes,[1] chemistry of NO mediated by free transition-metal atoms and ions has been reported. For example, reactions of neutral Sc, Ti and V atoms with a NO molecule were reported to form ScO, TiO and VO, respectively, by theory and experiment.[2–5] Similarly, cationic Ti^+ was found experimentally to produce TiO^+ through a reaction with a NO molecule.[6,7] Further reaction of TiO^+ with two NO molecules was reported by a theoretical study to produce TiO_2^+ along with N_2O.[8] In contrast to Sc and Ti, the reactivity of cationic iron, Fe^+, toward NO was reported to be very low, where only molecular adsorption of NO was observed.[9–12] It is reported also for cationic nickel, Ni^+, that NO is bound to Ni molecularly to form a nitrosyl nickel cation, $Ni(NO)_3^+$, as revealed by collision induced dissociation.[13] Infrared spectroscopy and theoretical studies revealed that NO is molecularly adsorbed on Cr^+, Mn^+, Fe^+, Co^+ and Ni^+ in an end-on configuration in their ground states.[14,15]

Gas-phase clusters consisting of a finite number of metal atoms and their compounds have been attracting much attention as model systems of heterogeneous catalysts, because of their unique size-dependent reactivity that cannot be expected from the properties of atoms and ions.[1,16] In this context, reactions of various metal clusters, e.g., Co_n^+,[17–21] Ni_n^-,[22] $Cu_n^{\pm/0}$,[23,24] $Nb_n^{\pm}$,[25] $Rh_n^{\pm}$,[26,27] and $Ag_n^{\pm}$,[28–30] with NO have been studied. $Cu_n^{\pm/0}$ are reported to adsorb NO although the reactivity is very low at any size.[23,24] On the other hand, Co_n^+ cluster ions, in contrast to the atomic Co^+ ion, exhibit dissociative adsorption of NO,[17,19] which is followed by release of N_2 to produce O_2 adducts.[20,21] Sequential adsorption of NO and release of N_2 have also been reported for $Rh_n^{\pm}$.[26,27] For Ni_n^- and Nb_n^-, production of NO_2^- and NO_3^- via electron transfer from the cluster was observed as well as release of N_2 forming oxidized cluster anions.[22,25] For Nb_n^+, formation of $Nb_nN_2O^+$ and $Nb_nNO_2^+$ were observed.[25] In addition to these reaction experiments, IR multiphoton dissociation spectroscopy is reported for Au_nNO^+ and Rh_nTaNO^+;[31,32] an odd–even oscillation was reported for the NO stretching frequency of Au_nNO^+.[31] Computational studies were performed for $Fe_nNO^{\pm}$,[33] $Rh_nNO^{\pm/0}$,[34] Pd_nNO^+,[35] and $Au_nNO^{\pm/0}$,[36,37] to obtain their geometric and electronic structures. Nitric oxide thus shows a rich variety of reactions depending on the reactant clusters.

Recently, a significant change in reactivity was reported for Cu_n^+ by doping an Al, Ti, or V atom.[38,39] NO molecules adsorbed on $Cu_n^{\pm/0}$ did not exhibit reaction between them,[23,24] whereas release of N_2 was observed for Cu_nAl^+.[38] As for Cu_nTi^+ and Cu_nV^+, it was reported that they release Cu atoms upon adsorption of a single NO molecule.[39] Reactions under multiple collision conditions were examined for Cu_7Ti^+, where formation of O adducts was observed

[a] Department of Chemistry, Faculty of Science, Kyushu University, 744 Motooka, Nishi-ku, Fukuoka 819-0395, Japan. E-mails: arakawa@chem.kyushu-univ.jp, terasaki@chem.kyushu-univ.jp

† Electronic Supplementary Information (ESI) available: Size-dependent mass spectra of product ions upon reaction of Ag_nM^+ with NO molecules for M = Ti, V, Mn, Fe, Co and Ni; reaction kinetics and pathways of Ag_nTi^+ with NO. See DOI: 10.1039/x0xx00000x

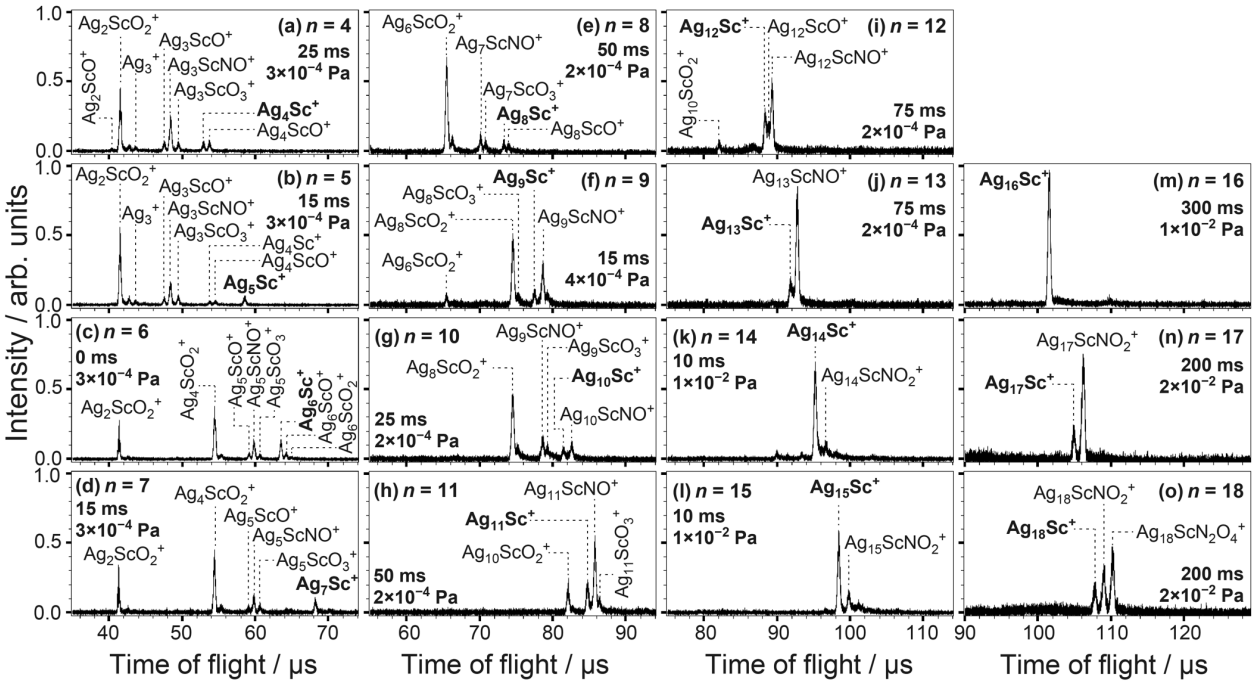

Fig. 1. Mass spectra of ions produced from Ag_nSc^+ reacting with NO molecules for n = 4–18 in panels a–o, respectively. The partial pressure of NO, P_{NO}, and the storage time, t, are given in each panel.

along with release of a N_2 molecule and Cu atoms.[39] These reactions show that a single heterogeneous metal atom opens various reaction channels when it is doped in metal clusters.

Multiple-collision experiment can be used to track successive elementary reaction processes.[40–46] We recently reported reaction kinetics of multiple NO molecules on Ag_n^+ clusters,[30] where two reaction mechanisms were found: (1) formation of $Ag_nNO_2^+$ via an intermediate Ag_nO^+; (2) direct formation of $Ag_nNO_2^+$ from Ag_n^+, implying NO disproportionation. Multiple NO adducts, $Ag_n(NO_2)_m^+$, were produced through successive reactions of (1) or (2). In the present study, we investigate Ag_nM^+ (M = Sc–Ni) interacting with NO to examine effects of doping of a 3d-transition-metal atom to Ag_n^+, focusing on size- and dopant-dependent reaction pathways as well as reaction rates.

2 Methods

The experimental setup has been described in detail elsewhere.[47] Briefly, Ag_nM^+ (M = Sc–Ni) were generated by a magnetron-sputter cluster-ion source,[48] where two metal target plates were cosputtered by placing a Ag plate (Toshima Manufacturing Co., Ltd.; 99.99%) with two 8-mm holes over a transition-metal plate (Kojundo Chemical Laboratory Co., Ltd., 99.99%). The sputtered atoms and ions were encouraged to form clusters in a buffer helium gas (99.99995%) cooled by liquid nitrogen. The cluster cations, thermalized by collisions with a helium gas at liquid-nitrogen temperature, were mass selected by a quadrupole mass filter (MAX-4000, Extrel CMS, LLC). Reactant cluster cations thus size-selected were guided by radio frequency (rf) octopole ion guides and quadrupole deflectors, and were admitted into a 30-cm-long linear quadrupole ion trap at a translational energy of ~10 eV in the laboratory frame. The ion trap was enclosed in a reaction gas cell, which was filled with a pressure-controlled NO gas along with a 0.3-Pa He gas at room temperature. The partial pressure of the reactant NO, P_{NO}, was adjusted in the range between 1×10^{-4} and 2×10^{-2} Pa so that the overall reaction came into the time window of the measurement. The partial pressures of He and NO gases were measured by a residual gas analyzer (RGA100, Stanford Research Systems, Inc.) outside the gas cell, which were converted to the pressure inside the gas cell, as reported previously,[49] by referring to the reaction cross sections of Co_n^+ with O_2.[50] A care was taken to prevent NO from reacting with a trace amount of residual gases of O_2 and H_2O, which would convert NO to NO_2; the partial pressure of NO_2 was less than 0.1% of that of NO as observed by the RGA. Reactant cluster cations were stored in the ion trap for a variable time, t, for reaction after ion loading for 50–200 ms. Ions of reaction products extracted from the ion trap were analyzed by a reflectron time-of-flight (TOF) mass spectrometer.[51,52] The yields of reactant and product ions were evaluated as a function of storage time t by accumulating 100 cycles of measurement at each storage time. The kinetics data were fitted to rate equations for analysis of reaction pathways by a program coded by referring to the DETMECH software,[53] i.e., rate constants of each reaction step were optimized by the least-squares method employing the Simplex algorithm so that fitting curves simulated using the Runge–Kutta–Nyström method reproduce the experimental data. All the possible reaction pathways were examined to search for the most probable one.

3 Results and Discussion

3.1 Reaction products.

We discuss M = Sc–V and Cr–Ni separately in subsections 3.1.1 and 3.1.2, respectively, according to their features in major product ions observed for small sizes.

Table 1. Sizes, *n*, for each size range classified by the major reaction products and the size of 18 electron clusters of Ag_nM^+ (M = Sc–V).

Size range	Major product	Sc	Ti	V
A	O adduct	4–12	3–11	3–10
B	NO adduct	13	12–13	11
C	NO_2 adduct	14–18	14–17	12–16
18e		16	15	14

3.1.1. Major reaction products for M = Sc–V. Figure 1 shows mass spectra of product ions upon reaction of Ag_nSc^+ with NO molecules for *n* = 4–18. The size, *n*, of the clusters is classified into three regions, as summarized in Table 1, according to major reaction products observed: size range A for O adducts, B for a NO adduct and C for NO_2 adducts. In size range A with $n \le 12$, O adducts are observed as major reaction products along with NO adducts, most of which are accompanied by Ag dissociation at smaller sizes. For example, Ag_4Sc^+ produces Ag_2ScO^+, $Ag_2ScO_2^+$, Ag_3^+, Ag_3ScO^+, Ag_3ScNO^+, $Ag_3ScO_3^+$ and Ag_4ScO^+ as shown in Fig. 1a; these products have an even number of electrons except for Ag_3ScO^+ and $Ag_3ScO_3^+$. Note that the final products are $Ag_{n'}ScO_2^+$ with even electrons, i.e., with even n' ($n' < n$), as is manifested by reaction kinetics discussed in subsection 3.3. The result for size range A is in contrast to that of undoped Ag_n^+, where NO_2 adducts, $Ag_n(NO_2)_m^+$, are mainly observed,[30] suggesting that the Sc atom provides an active site; a large binding energy of NO to the Sc atom would have induced substantial dissociation. Formation of oxygen adducts resembles the nature of the transition-metal atom as reported for a neutral Sc atom to produce ScO by reaction with a NO molecule.[2–4]

In size range B, i.e., at *n* = 13, a simple NO adduct $Ag_{13}ScNO^+$ is produced without dissociation. The result implies that oxidation did not proceed because only one NO molecule was able to approach the active Sc site due to almost full encapsulation by Ag atoms. It is speculated for the Ag_nSc^+ clusters that at least two NO molecules are required for oxide formation, which is in contrast to the behavior of the Sc atom forming ScO by a single NO molecule.[2–4]

In size range C with $n \ge 14$, major reaction products are NO_2 adducts, $Ag_nSc(NO_2)_m^+$, which is similar to the result of undoped Ag_n^+.[29,30] The products suggest that the reaction site changes from Sc to Ag when the Sc atom is fully encapsulated by Ag atoms. Note that no reaction products were observed for $Ag_{16}Sc^+$, which possesses 18 valence electrons from Ag $5s^1$, Sc $4s^2$, Sc $3d^1$ and a positive charge. The minimum reactivity indicates that a closed electronic shell was formed by the 18 electrons via delocalization of the 3d electron of Sc. The reduced reactivity of $Ag_{16}Sc^+$ was also observed in its reaction with O_2.[47]

The features in the reaction products observed upon Sc doping described above are common to M = Ti and V as shown in Figs. S1 and S2, respectively, in the ESI. The size ranges categorized by the major reaction products are added in Table 1 for M = Ti and V as well. For Ag_nTi^+, size range A is identified as $n \le 11$, where O adducts are observed as major reaction products, along with minor products including NO adducts and Ti-free Ag cluster cations. It is common for these small sizes that dissociation channels are dominant. It is noted that the major products have an even number of electrons as shown in Fig. S1, i.e., Ag^+, Ag_3^+ and $AgTiO_2^+$ for *n* = 3–5, Ag^+, Ag_3^+, $Ag_3TiO_2^+$, Ag_4TiNO^+ and $Ag_4TiNO_2^+$ for *n* = 6, $Ag_3TiO_2^+$ and $Ag_5TiO_2^+$ for *n* = 7,

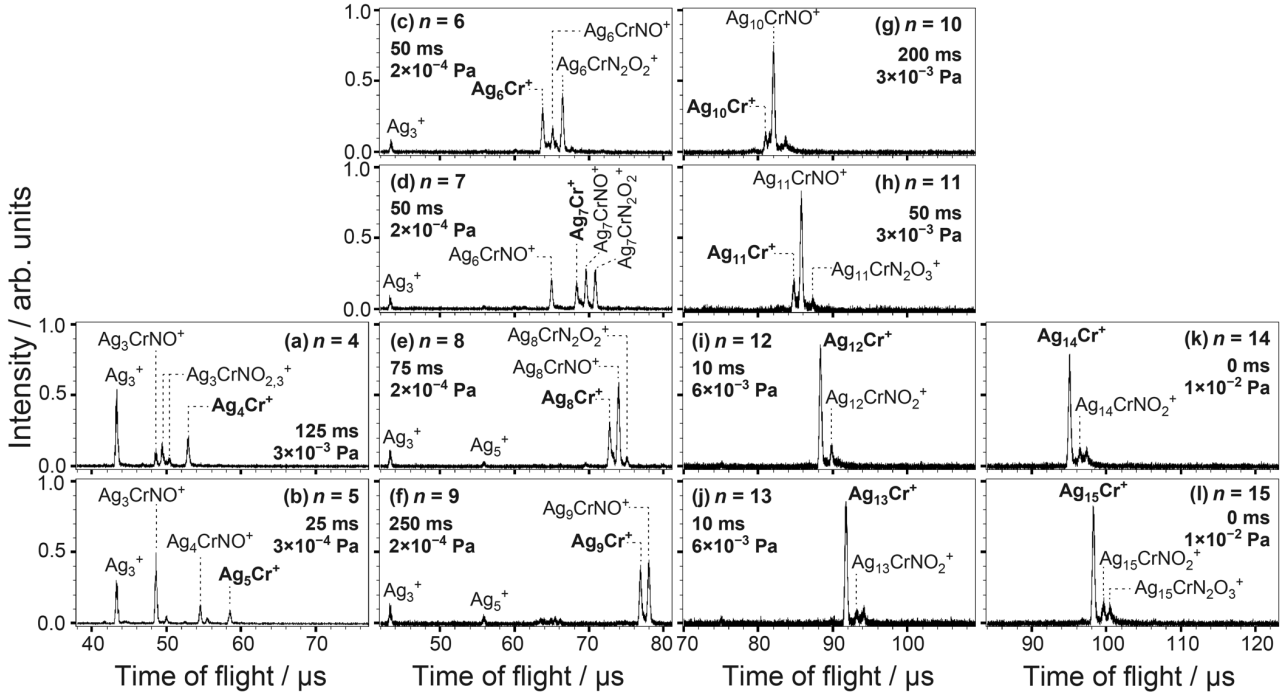

Fig. 2. Mass spectra of ions produced from Ag_nCr^+ reacting with NO molecules for *n* = 4–15 in panels a–l, respectively. The partial pressure of NO, P_{NO}, and the storage time, *t*, are given in each panel.

$Ag_5TiO_2^+$ for n = 8, $Ag_7TiO_2^+$ for n = 9, $Ag_8TiNO_3^+$ for n = 10 and $Ag_{10}TiNO^+$ for n = 11. Note also that the final products are not always ions with even electrons as will be discussed in subsection 3.3. Formation of oxygen adducts is similar to those reported for a neutral Ti atom and a cationic Ti^+ to produce TiO and TiO^+, respectively, by reaction with a single NO.[5–8]

The size range B is assignable to n = 12 and 13, where a simple NO adduct, $Ag_{12}TiNO^+$ and $Ag_{13}TiNO^+$, respectively, is the only product ions; only one NO molecule approaches the active Ti site due to almost full encapsulation by Ag atoms. It is speculated that at least two NO molecules are required for oxidation of the cluster as in the case of M = Sc. The size range C is found at larger sizes, $n \geq 14$, where major reaction products are NO_2 adducts. This similarity to the reaction channels of undoped Ag_n^+ indicates that the reaction site changes from Ti to Ag when the Ti atom is fully encapsulated by Ag atoms as also in the case of M = Sc.

As for Ag_nV^+, O adducts accompanied by dissociation dominated the product ions up to n = 10, which are classified as size range A. The size n = 11 is recognized as size range B, where a simple NO adduct $Ag_{11}VNO^+$ was the only product. Formation of $Ag_nV(NO_2)_m^+$ was the dominant pathways at $14 \leq n \leq 16$, which allows us to assign size range C, indicating a change in the reaction site from the V atom to a Ag atom. We categorize n = 12 and 13 as size range C, even though O adducts were observed dominantly; these O adducts are dissociation free and, therefore, might be intermediates for NO_2 adducts on the Ag sites.

3.1.2 Major reaction products for M = Cr–Ni. Similarly to M = Sc–V, three size ranges were identified again according to major reaction products observed, which are summarized in Table 2: size range B for a single NO adduct and C for NO_2 adducts. The sizes smaller than size range B were categorized as size range A, which is featured by multiple NO adducts although adsorption of only one or no NO molecule is discernible at very small sizes probably due to considerable dissociation processes. Note that size range A is characterized by product ions significantly different from the O adducts observed in the case of M = Sc–V.

Figure 2 shows mass spectra of product ions upon reaction of Ag_nCr^+ (n = 4–15) with NO molecules. Size range A is assignable to $n \leq 8$. Multiple NO adducts dominated the products for n = 6–8, while single NO adducts were produced for n = 4 and 5; O adducts were not observed in contrast to M = Sc–V. For example, Ag_7Cr^+ produces Ag_3^+, Ag_6CrNO^+, Ag_7CrNO^+ and $Ag_7Cr(NO)_2^+$. Ag_3^+ was observed commonly for n = 4–9. Dissociation would have been induced by an adsorption energy of NO to the active Cr site. The branching ratio of the dissociative channels was lower than that of M = Sc–V, which might be due to a lower adsorption energy. No preference was observed for even-electron systems. In size range B (n = 9–11), a single-NO adduct, Ag_nCrNO^+, is the major reaction product. At n = 11, a small peak is observed at $Ag_{11}CrN_2O_3^+$ (i.e., $Ag_{11}CrNO(NO_2)^+$) along with the major product, $Ag_{11}CrNO^+$; the NO molecule may be adsorbed on the Cr site and the NO_2 molecule on a Ag site. The NO_2 adducts become major for $n \geq 12$, which are categorized as size range C. The size-dependent change in the major products suggests that the reaction site changed from Cr to Ag in the course of encapsulation.

The features in the reaction products observed for M = Cr described above were common to M = Mn, Fe, Co and Ni as shown in Figs. S3, S4, S5 and S6, respectively, in the ESI. The size ranges classified by the major reaction products are summarized in Table 2 for M = Cr–Ni. For all these doped clusters, NO adducts were formed for small sizes defined as size range A. The branching ratio of dissociation was low as pointed out for M = Cr. Furthermore, the window of size range A is much smaller than those for M = Sc–V. For larger sizes, reaction products changed from a single-NO adduct to NO_2 adducts as assigned to size range C.

The formation of NO adducts in size range A resembles the nature of the atoms of these transition-metal elements. For example, cationic iron, Fe^+, is reported to show very low reactivity toward NO, where only molecular adsorption of NO was observed.[9–12] Similarly, it was reported for cationic nickel, Ni^+, that NO is bound to Ni molecularly to form a nitrosyl nickel cation, $Ni(NO)_3^+$.[13] A spectroscopic study reported that NO molecules are molecularly adsorbed on $Co^{0/+}$ as well as $Fe^{0/+}$ and $Ni^{0/+}$.[14] Note that the reaction products from the pure cobalt cluster, Co_n^+, is different from those from Ag_nCo^+ and Co^+; sequential dissociative adsorption of NO on Co_n^+ is followed by a release of N_2 to produce O_2 adducts.[19–21] This implies that the reduction of NO requires two or more Co atoms.

3.1.3 Other features. As described in subsections 3.1.1 and 3.1.2, O adducts, NO adducts and dopant-free Ag clusters were produced for small size ranges A and B. The ions with an even number of electrons were observed preferentially for dopant-free Ag clusters as well as for O adducts mentioned above. For example, Ag^+ was produced predominantly for $Ag_{3–5}Ti^+$ and Ag_3V^+, whereas Ag_3^+ was favorable for Ag_6Ti^+, $Ag_{3–7}V^+$, $Ag_{4–9}Cr^+$, $Ag_{3–5}Mn^+$, Ag_4Fe^+, Ag_4Co^+ and Ag_4Ni^+. The preferential formation of Ag^+ and Ag_3^+ can be attributed to the stability of the even-electron systems. As for NO adducts, preference for even electrons was not observed clearly, which implies that interaction between clusters and an adsorbent NO molecule is weak.

On the other hand, the stability of the ions with 18 valence electrons is manifested as the reactivity minima in the size dependence, which will be discussed in subsection 3.2. In spite of their stability, most of them were not observed as a reaction product. This is because all the Ag_nM^+ clusters with 18 valence electrons, belong to size range C, where dissociation is a minor reaction channel. An exception is Ag_nNi^+, where 18-valence electron cluster, Ag_9Ni^+, was produced as one of the two major products in the

Table 2. Sizes, n, for each size range classified by the major reaction products and the size of 18 electron clusters of Ag_nM^+ (M = Cr–Ni).

Size range	Major product	Cr	Mn	Fe	Co	Ni
A	$(NO)_m$ adduct (m = 0–3)	4–8	3–6	3–6	3–6	3–5
B	single NO adduct	9–11	7–10	7–9	7–8	6–9
C	NO_2 adduct	12–15	11–15	10–14	9–14	10–14
18e		13	12	11	10	9

reaction of $Ag_{10}Ni^+$ (see Fig. S7h). Formation of Ag_9Ni^+ is attributed ~~to~~ both to its exceptional stability and to the fact that $Ag_{10}Ni^+$ is at the boundary between size ranges B and C, exhibiting both dissociative reaction and formation of NO_2 adducts.

3.2 Reactivity evaluated by extinction rates of reactant.

The extinction rate coefficient, k, of reactant, Ag_nM^+, was evaluated to show size dependence of reactivity in the same way as reported for the reaction with O_2;[47] the extinction rate constant of the reactant cluster was divided by the number density of NO in the ion trap under the assumption that the elementary reaction is the first order for NO. The size-dependent reaction rate coefficients of Ag_nM^+ thus obtained are plotted in Fig. 3 along with those of undoped Ag_n^+ previously measured;[30] they show relative values with respect to the rate coefficient of Ag_8^+ reacting with O_2, $(6 \pm 2) \times 10^{-15}$ $cm^3\ s^{-1}$,[30] so that the coefficients of Ag_nM^+ reacting with NO can be compared with those of Ag_n^+ and Ag_nM^+ reacting with O_2 previously reported.[30,47] Note that reaction rate coefficients are subject to a systematic error of about 30% mainly due to uncertainty in the pressure of the reactant gas in the ion trap; Fig. 3 displays relative values, which only have a statistical error of about 5%, to show the size dependence clearly. The value $<10^{-1}$ indicates that no product was observed with the present sensitivity of ion detection. Size ranges A, B and C categorized by the reaction products are shown as well, which are in good correlation with the reactivity as described below.

Fig. 3a shows the result of Ag_nSc^+. In size range A, the rate coefficients are more than two orders of magnitude higher than that of undoped Ag_n^+, implying that the presence of a Sc atom strongly enhances the reactivity. In size range B, the reactivity decreases but is higher than that of undoped Ag_n^+. The reactivity is further reduced in size range C, which is even slightly lower than that of Ag_n^+. The size-dependent reactivity as well as the chemical composition of the product ions indicate a change in the active site from Sc to Ag when the Sc atom is covered with Ag atoms as the size increases. In addition to the decrease in reactivity upon encapsulation of the Sc atom, a reactivity minimum is observed at n = 16 (the solid arrow in Figure 3a), which has 18 valence electrons including a 3d electron. The minimum reactivity provides an evidence for enhanced stability of $Ag_{16}Sc^+$.

The most of these features in the size-dependent reactivity of Ag_nSc^+ are common to other dopant elements as shown in Fig. 3. Size range C starts at n = 14, 14, 12, 12, 11, 10, 9 and 10 for M = Sc, Ti, V, Cr, Mn, Fe, Co and Ni, respectively; the critical size for encapsulation of the dopant atom has a decreasing trend as the atomic number increases from Sc to Ni. This is consistent with the previous result for the reaction with O_2; the critical size depends on the atomic radius of the dopant that governs the least number of Ag atoms for encapsulation.[47] This effect of encapsulation on lowering reactivity is analogous to that previously reported for transition-metal-doped Si clusters.[54–56]

The cluster size with 18 valence electrons is indicated by the solid arrow in each panel of Fig. 3. A reactivity minimum was observed at the 18-valence-electron system for M= Sc, Ti, V and Ni. This is consistent with the reactivity toward O_2 previously reported;[47] note

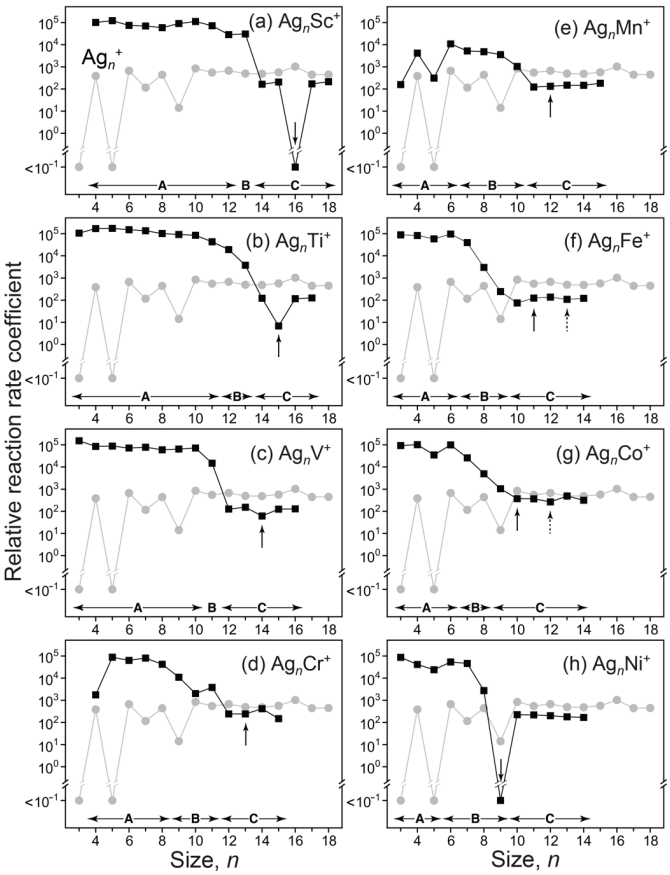

Fig. 3. Size dependence of reaction rate coefficients of Ag_nM^+ toward NO; M = (a) Sc, (b) Ti, (c) V, (d) Cr, (e) Mn, (f) Fe, (g) Co and (h) Ni. The rate coefficients of undoped Ag_n^+ are superimposed in each panel in gray.[30] The rate coefficients are relative values with respect to that of Ag_8^+ reacting with O_2, which is reported to be $(6 \pm 2) \times 10^{-15}$ cm^3s^{-1}.[47] The value $<10^{-3}$ indicates that no product was observed with the present sensitivity of ion detection.

that the reactivity minima in the present study is more prominent. The results suggest that $Ag_{16}Sc^+$, $Ag_{15}Ti^+$, $Ag_{14}V^+$ and Ag_9Ni^+ form a closed electronic shell with 18 electrons by delocalized 3d electrons along with s electrons of the dopant and the host atoms. The shell closure at the 18-valence-electron system is consistent with the previous studies by photofragmentation,[57,58] theoretical calculation,[59–66] and chemical reaction with O_2.[47,67,68]

On the other hand, the reactivity minimum was not observed clearly for M = Cr, Mn, Fe and Co. The missing reactivity minimum at $Ag_{13}Cr^+$ and $Ag_{12}Mn^+$ can be explained by the half-filled nature of the d orbital as discussed in the previous studies.[47,56] As for M = Fe and Co, the minimum was observed at a size with 20 valence electrons rather than 18 as indicated by dashed arrows in Figs. 3f and 3g. The reactivity was rather lower at n = 10 with 17 valence electrons for M = Fe. This is in contrast to the result previously reported for the reaction with O_2, where the reactivity minimum was clearly observed for 18 as well as 20-electron systems.[47] We currently have no explanation on this dip at $Ag_{10}Fe^+$ in the reaction with NO.

3.3 Reaction kinetics.

Here we discuss reaction kinetics for M = Sc and Ti focusing on formation of oxygen adducts in the small size ranges A and B, where

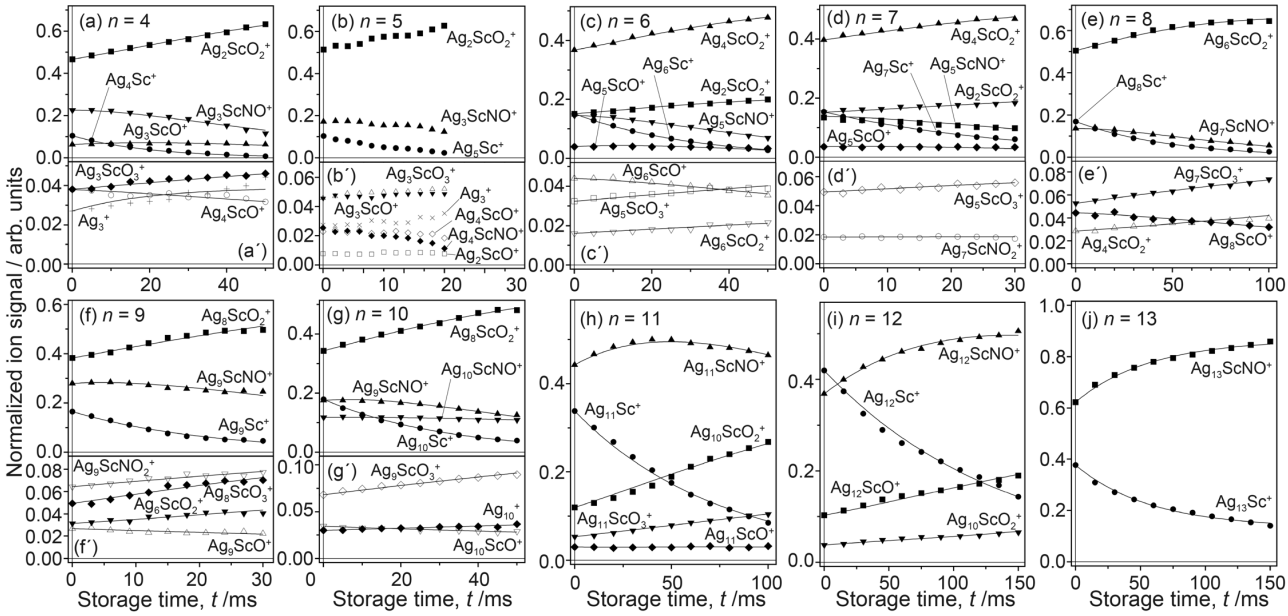

Fig. 4. Reaction kinetics of Ag_nSc^+ interacting with NO. (a)–(j) for n = 4–13, respectively. For n =4–9, minor products are displayed in a magnified scale in a'–g'. The ion signals are normalized so that the total signal of the entire ions is unity at each storage time. Fitting curves are superimposed by solid lines, except for n = 5; the experimental result of n = 5 did not provide reliable rate constants. P_{NO} was 3 × 10^{-4} Pa for n = 4–7, 2 × 10^{-4} Pa for n = 8, 10–13 and 4 × 10^{-4} Pa for n = 9.

a wide variety of product ions were generated by the active Sc or Ti sites. Note that the results in size range C did not provide reliable reaction pathways because of the low data quality of weak product-ion signals; the NO_2 adducts observed in size range C might be produced by the same pathways as reported for Ag_n^+.[30]

Figure 4 shows temporal evolution of ion signals of the reactant and products as a function of storage time, t, for Ag_nSc^+ with n = 4–13. The ion signal is defined as a fraction of each ion in the entire ions observed. Each panel was obtained by analyzing a series of TOF mass spectra measured as a function of storage time of the reactant cluster ion. Note that product ions were observed already at t = 0, which were produced during ion loading to the ion trap.

For n = 4 (Figs. 4a and 4a'), the reactant Ag_4Sc^+ disappears exponentially with the storage time, while product ions are formed accordingly. As for major products shown in panel (a), the ion signal of Ag_3ScNO^+ is followed by Ag_3ScO^+, which is further transformed to produce $Ag_2ScO_2^+$ eventually. As for minor products shown in panel (a'), $Ag_3ScO_3^+$ and Ag_3^+ increase with the storage time, while Ag_4ScO^+ decreases.

The reaction pathway to form these product ions was identified by fitting the data to rate equations, where possible reaction pathways were examined to search for the most probable one. The present reactions take place in a pseudo-first-order process because the reaction cell enclosing the ion trap was filled with NO and He gases at constant partial pressures much higher than the corresponding density of the reactant ions, Ag_4Sc^+. The solid lines in Figs. 4a and 4a' show data fitting to rate equations. The best fit was obtained for the following differential equations, which are based on the reaction pathway shown in Scheme 1:

$$d[Ag_4Sc^+]/dt = -(k_{4,1} + k_{4,4} + k_{4,5})[Ag_4Sc^+] \quad (1)$$

$$d[Ag_3ScNO^+]/dt = k_{4,1}[Ag_4Sc^+] - k_{4,2}[Ag_3ScNO^+] \quad (2)$$

$$d[Ag_3ScO^+]/dt = k_{4,2}[Ag_3ScNO^+] - k_{4,3}[Ag_3ScO^+] \quad (3)$$

$$d[Ag_2ScO_2^+]/dt = k_{4,3}[Ag_3ScO^+] \quad (4)$$

$$d[Ag_3^+]/dt = k_{4,4}[Ag_4Sc^+] \quad (5)$$

$$d[Ag_4ScO^+]/dt = k_{4,5}[Ag_4Sc^+] - k_{4,6}[Ag_4ScO^+] \quad (6)$$

$$d[Ag_3ScO_3^+]/dt = k_{4,6}[Ag_4ScO^+]. \quad (7)$$

The pseudo-first-order rate constants of each step of elementary reactions, $k_{4,1}$, $k_{4,2}$, $k_{4,3}$, $k_{4,4}$, $k_{4,5}$ and $k_{4,6}$ are obtained to be 42.9, 19.1, 53.2, 5.7, 0.9, 4.5 s^{-1}, respectively. $Ag_2ScO_2^+$ is produced as a major product via the intermediates Ag_3ScNO^+ and Ag_3ScO^+: Ag_3ScNO^+ is produced from Ag_4Sc^+ in the first step, which is associated with a release of a neutral Ag atom. Ag_3ScNO^+ further reacts with a NO molecule to produce Ag_3ScO^+ along with N_2O, which was finally transformed to $Ag_2ScO_2^+$ with even electrons by further reaction. Thus, an oxygen adduct, $Ag_2ScO_2^+$, is formed as a major product ion, via multiple collisions with NO molecules. As for the minor products, $Ag_3ScO_3^+$ is produced via Ag_4ScO^+, while Ag_3^+ is produced directly from Ag_4Sc^+.

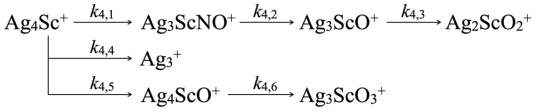

Scheme 1. Reaction pathways of Ag_4Sc^+ exposed to NO molecules. The parameters, $k_{4,x}$ (x = 1–6), represent reaction rate constants of each step at P_{NO} = 3 × 10^{-4} Pa.

The analysis of kinetics was carried out in the same way for all other sizes from n = 6 through 13. Solid curves in each panel of Fig. 4, except for n = 5, show the best fit to pseudo-first-order rate equations based on the reaction pathways shown in Scheme 2. The obtained pseudo-first-order reaction rate constants are given in the unit of s^{-1} for each step. Note that the result of Ag_5Sc^+ did not provide reliable rate constants because of the low data quality. In most cases of size range A, i.e., $n \le 12$, O adducts, $Ag_{n''}ScO_m^+$ ($n'' \le n$), are formed via an intermediate, $Ag_{n'}ScNO^+$ ($n'' \le n' \le n$). In particular, for n = 8–11, $Ag_{n''}ScO_2^+$ is formed from $Ag_{n'}ScNO^+$, where $Ag_{n''}ScO^+$ is not an intermediate for $Ag_{n''}ScO_2^+$; the result implies that O_2 adducts

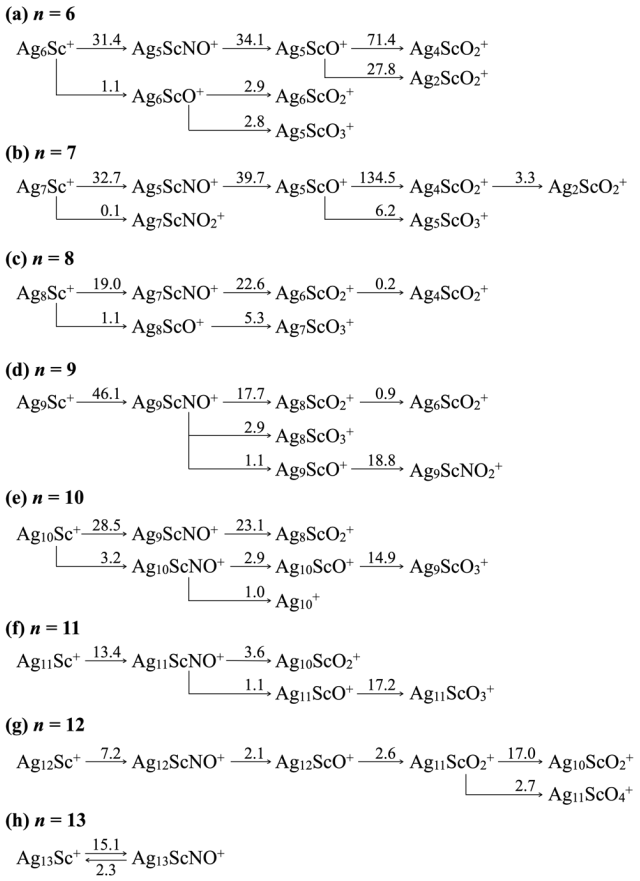

Scheme 2. Reaction pathways of Ag_nSc^+ reacting with NO molecules for n = 6–13. Reaction rate constants are given in the unit of s^{-1}. P_{NO} is 3 × 10^{-4} Pa for n = 6 and 7, 2 × 10^{-4} Pa for n = 8, 10–13 and 4 × 10^{-4} Pa for n = 9.

are formed via the reaction between $Ag_{n'}ScNO^+$ and NO with a release of a N_2 molecule as well as Ag atom(s). The final products are $Ag_{n'}ScO_2^+$ with even electrons, i.e., with even n' ($n' < n$), which suggest the stability of the even-electron systems. As for size range B of n = 13, $Ag_{13}Sc^+$ and $Ag_{13}ScNO^+$ are in equilibrium, which indicates that the NO molecule physisorbed on $Ag_{13}Sc^+$ repeats an adsorption–dissociation cycle.

The analysis of kinetics was also carried out for Ag_nTi^+ in the size range A (n = 3–11), which is shown in Fig. S7 and Scheme S1 of the ESI. The reaction pathways are more complex than those of Ag_nSc^+ because a wide variety of product ions generated by dissociative reactions were observed in a broad mass range. The final products were O adducts, $Ag_{n''}TiO_m^+$ ($n'' \le n$), as in the case of Ag_nSc^+. In addition to O adducts, $Ag_{n''}^+$ and $Ag_{n''}TiNO_m^+$ were among the final products; in particular, a larger amount of $Ag_{n''}^+$ was observed compared to the case of Ag_nSc^+. The O adducts, $Ag_{n''}TiO_m^+$ ($n'' \le n$), are formed via an intermediate, $Ag_{n'}TiNO^+$ ($n'' \le n' \le n$), as in the case of Ag_nSc^+. In most cases, $Ag_{n''}TiO_2^+$ is formed from $Ag_{n'}TiNO^+$ not via $Ag_{n''}TiO^+$, as pointed out for n = 8–11 of Ag_nSc^+. This reaction pathway to produce an O_2 adduct is different from that for the atomic Ti^+ reported theoretically, where three NO molecules reacting with Ti^+ produce TiO_2^+ along with N and N_2O via TiO^+ and $TiNO_2^+$.[8] The present result is rather similar to those of Ti-doped Cu cluster cations, where reaction with two NO molecules produces an O_2 adduct with a release of a N_2 molecule.[39] The results imply that the reactivity of the transition-metal atom is modified by the host Ag or Cu atoms. As for size range B (n = 12 and 13), while Ag_nTi^+ was transformed to Ag_nTiNO^+ for n = 12, Ag_nTi^+ and Ag_nTiNO^+ are in equilibrium for n = 13. This is attributed to screening of the Ti site by the host Ag atoms, which reduces an adsorption energy of NO.

Conclusions

We investigated gas-phase reaction kinetics and reactivity of free Ag_nM^+ (M = Sc−Ni) clusters interacting with NO molecules by employing an ion trap. Size-dependent reactivity exhibited features similar to those observed for their reaction with O_2 reported previously: small sizes are highly reactive, which implies that the 3d-transition-metal dopant strongly enhances the reactivity by providing an active site. The reactivity showed a significant drop at a critical size in accordance with encapsulation of the dopant atom; the active site is altered to the Ag host. Except for M = Cr and Mn, the reactivity reached a minimum at a specific size, where the cluster cation possesses 18 or 20 valence electrons with 3d and 4s of the dopant as well as Ag 5s. We focused also on size-dependent formation of reaction products due to the change in the active site. For Ag_nM^+ doped with a late-transition-metal atom, M = Cr–Ni, the product ions changed from NO adducts, $Ag_nM(NO)_m^+$, to NO_2 adducts, $Ag_nM(NO_2)_m^+$, as the size increased. On the other hand, doping of an early-transition-metal atom, Sc, Ti, or V, opened reaction channels to O adducts in the small size range. The product ions changed from the O adducts to NO adducts as the size increased, to NO_2 adducts, $Ag_nM(NO_2)_m^+$, at larger sizes with the dopant atom encapsulated by the Ag host. The products in the small size range, i.e., either O adducts or NO adducts, are similar to those produced from the corresponding transition-metal atom, while the formation of $Ag_nM(NO_2)_m^+$ at large sizes mimics the reaction of undoped silver clusters, Ag_n^+, that produce $Ag_n(NO_2)_m^+$. Kinetics measurements on Ag_nSc^+ and Ag_nTi^+ further revealed that O adducts in the small size range are formed via NO adducts; the pathway is different from that has been reported for the atomic cation Ti^+. The present study thus showed a variety of reaction channels of transition-metal ions interacting with NO that can be tuned by clustering with Ag atoms.

Author Contributions

M. A. contributed to Conceptualization, Investigation, Formal analysis, Writing - original draft and Funding acquisition. M. H. contributed to Investigation and Formal analysis. K. M. and T. K. contributed to Investigation. A. T. contributed to Conceptualization, Writing - review & editing, Supervision, Project administration and Funding acquisition.

Conflicts of Interest

There are no conflicts to declare.

Acknowledgements

The present study was supported by Grants-in-Aid for Scientific Research (A) (JP18H03901) and for Scientific Research (C)

(JP19K05185) from the Japan Society for Promotion of Science (JSPS), and for Scientific Research on Innovative Areas (JP17H06456) from the Ministry of Education, Culture, Sports, Science and Technology (MEXT).

References

1 D. K. Böhme and H. Schwarz, Gas-phase catalysis by atomic and cluster metal ions: The ultimate single-site catalysts, *Angew. Chem. Int. Ed.*, 2005, **44**, 2336–2354.

2 D. Ritter and J. C. Weisshaar, Kinetics of neutral transition-metal atoms in the gas phase: Oxidation of Sc (a^2D), Ti (a^3F), and V (a^4F) by NO, O_2, and N_2O, *J. Phys. Chem.*, 1990, **94**, 4907−4913.

3 K. H. Kim, Y. S. Lee, D. K. Kim, K. S. Kim and G.-H. Jeung, Theoretical study of the gas phase Sc + (NO, O_2) → ScO + (N, O) reactions, *J. Phys. Chem. A*, 2002, **106**, 9600–9605.

4 K. H. Kim, Y. S. Lee, J.-H. Moon and G.-H. Jeung, Theoretical study of the Ti + (NO, O_2) → TiO + (N, O) reactions, *J. Chem. Phys.*, 2002, **117**, 8385–8390.

5 G.-H. Jeung, P. Luc, R. Vetter, K. H. Kim and Y. S. Lee, Experimental and theoretical study on the reaction Sc + NO → ScO + N, *Phys. Chem. Chem. Phys.*, 2002, **4**, 596–600.

6 R. Johnsen, F. R. Castell and M. A. Biondi, Rate coefficients for oxidation of Ti^+ and Th^+ by O_2 and NO at low energies, *J. Chem. Phys.*, 1974, **61**, 5404–5407.

7 M. M. Kappes and R. H. Staley, Oxidation of transition-metal cations in the gas phase. Oxygen bond dissociation energies and formation of an excited-state product, *J. Phys. Chem.*, 1981, **85**, 942–944.

8 Z. Safaei and A. Shayesteh, Ab Initio calculations on sequential reactions of nitric oxide with titanium ions in the gas phase, *J. Phys. Chem. A*, 2020, **124**, 5194–5203.

9 J. V. B. Oriedo and D. H. Russell, Ion−molecule reaction chemistry of Fe^+ with NO: Excited-versus ground-state reactions, *J. Am. Chem. Soc.*, 1993, **115**, 8376−8381.

10 V. Baranoc, G. Jacahery, A. C. Hopkinson and D. K. Bohme, Intrinsic coordination properties of iron in FeO^+: Kinetics at 294 ± 3 K for gas-phase reactions of the ground states of Fe^+ and FeO^+ with inorganic ligands containing hydrogen, nitrogen, and oxygen, *J. Am. Chem. Soc.*, 1995, **117**, 12801–12809.

11 J. J. Melko, S. G. Ard, J. A. Fournier, N. S. Shuman, J. Troe and A. A. Viggiano, Exploring the reactions of Fe^+ and FeO^+ with NO and NO_2, *J. Phys. Chem. A*, 2012, **116**, 11500–11508.

12 L. Wang, G. Wang, H. Qu, C. Wang and M. Zhou, Infrared photodissociation spectroscopy of iron nitrosyl cation complexes: $Fe(NO)_n^+$ (n = 1–5), *J. Phys. Chem. A*, 2014, **118**, 1841–1849.

13 F. A. Khan, D. L. Steele and P. B. Armentrout, Ligand effects in organometallic thermochemistry: The sequential bond energies of $Ni(CO)_x^+$ and $Ni(N_2)_x^+$ (x = 1–4) and $Ni(NO)_x^+$ (x = 1–3), *J. Phys. Chem.*, 1995, **99**, 7819–7828.

14 M. Zhou and L. Andrews, Reactions of laser-ablated Fe, Co, and Ni with NO: Infrared spectra and density functional calculations of MNO^+ and $M(NO)_x$ (M = Fe, Co, x = 1–3; M = Ni, x = 1, 2), and $M(NO)_x^-$ (M = Co, Ni; x = 1, 2), *J. Phys. Chem. A*, 2000, **104**, 3915–3925.

15 J. L. C. Thomas, C. W. Bauschlicher, Jr. and M. B. Hall, Binding of nitric oxide to first-row transition metal cations: An *ab Initio* study. *J. Phys. Chem. A*, 1997, **101**, 8530–8539.

16 S. M. Lang, T. M. Bernhardt, Gas phase metal cluster model systems for heterogeneous catalysis, *Phys. Chem. Chem. Phys.*, 2012, **14**, 9255−9269.

17 J. J. Klaassen and D. B. Jacobson, Dissociative versus molecular chemisorption of nitric oxide on small bare cationic cobalt clusters in the gas phase, *J. Am. Chem. Soc.*, 1988, **110**, 974–976.

18 T. Hanmura, M. Ichihashi, Y. Watanabe, N. Isomura, T. Kondow, Reactions of nitrogen monoxide on cobalt cluster ions: Reaction enhancement by introduction of hydrogen, *J. Phys. Chem. A*, 2007, **111**, 422–428.

19 T. Hanmura, M. Ichihashi, R. Okawa and T. Kondow, Size-dependent reactivity of cobalt cluster ions with nitrogen monoxide: Competition between chemisorption and decomposition of NO, *Int. J. Mass Spectrom.*, 2009, **280**, 184–189.

20 M. L. Anderson, A. Lacz, T. Drewello, P. J. Derrick, D. P. Woodruff and S. R. Mackenzie, The chemistry of nitrogen oxides on small size-selected cobalt clusters, Co_n^+, *J. Chem. Phys.*, 2009, **130**, 064305.

21 K. Koyama, S. Kudoh, K. Miyajima and F. Mafuné, Thermal desorption spectroscopy study of the adsorption and reduction of NO by cobalt cluster ions under thermal equilibrium conditions at 300 K, *J. Phys. Chem. A*, 2015, **119**, 9573–9580.

22 W. D. Vann, R. L. Wagner and A. W. Castleman, Jr., Gas-phase reactions of nickel and nickel-rich oxide cluster anions with nitric oxide. 2. The addition of nitric oxide, oxidation of nickel clusters, and the formation of nitrogen oxide anions, *J. Phys. Chem. A*, 1998, **102**, 8804–8811.

23 L. Holmgren, M. Andersson and A. Rosén, NO on copper clusters, *Chem. Phys. Lett.*, 1998, **296**, 167–172.

24 S. Hirabayashi and M. Ichihashi, Reactions of size-selected copper cluster cations and anions with nitric oxide: enhancement of adsorption in coadsorption with oxygen, *J. Phys. Chem. A*, 2014, **118**, 1761–1768.

25 Q. Wu and S. Yang, Reactions of niobium cluster ions $Nb_x^±$ (x = 2–16) with NO and NO_2, *Int. J. Mass Spectrom.*, 1999, 184, 57–65.

26 M. S. Ford, M. L. Anderson, M. P. Barrow, D. P. Woodruff, T. Drewello, P. J. Derricka and S. R. Mackenzie, Reactions of Nitric Oxide on Rh_6^+ Clusters: Abundant chemistry and evidence of structural isomers, *Phys. Chem. Chem. Phys.*, 2005, **7**, 975–980.

27 M. L. Anderson, M. S. Ford, P. J. Derrick, T. Drewello, D. P. Woodruff and S. R. Mackenzie, nitric oxide decomposition on small rhodium clusters, $Rh^{+/-}$, *J. Phys. Chem. A*, 2006, 110, 10992–11000.

28 J. Hagen, L. D. Socaciu-Siebert, J. Le Roux, D. Popolan, S. Vajda, T. M. Bernhardt and L. Wöste, Charge transfer initiated nitroxyl chemistry on free silver clusters Ag_{2-5}^-: size effects and magic complexes, *Int. J. Mass Spectrom.*, 2007, **261**, 152–158.

29 J. Ma, X. Cao, J. Liu, B. Yin and X. Xing, The adsorption and activation of NO on silver clusters with sizes up to one nanometer: Interactions dominated by electron transfer from silver to NO, *Phys. Chem. Chem. Phys.*, 2016, **18**, 12819–12827.

30 M. Arakawa, M. Horioka, K Minamikawa, T. Kawano and A. Terasaki, Size-dependent reaction kinetics of silver cluster cations with nitric oxide, *J. Phys. Chem. C*, 2020, **124**, 26881–26888.

31 A. Fielicke, G. von Helden, G. Meijer, B. Simard and D. M. Rayner, Direct observation of size dependent activation of NO on gold clusters, *Phys. Chem. Chem. Phys.*, 2005, **7**, 3906–3909.

32 M. Yamaguchi, S. Kudoh, K. Miyajima, O. V. Lushchikoca, J. M. Bakker, F. Mafuné, Tuning the dissociative action of cationic Rh clusters toward NO by substituting a single Ta atom, *J. Phys. Chem. C*, 2019, **123**, 3476–3481.

33 G. L. Gutsev, M. D. Mochena, E. Johnson and C. W. Bauschlicher, Dissociative and associative attachment of NO to iron clusters, *J. Chem. Phys.*, 2006, **125**, 194312.

34 A. Dutta and P. A. Mondal, Density functional study on the electronic structure, nature of bonding and reactivity of NO adsorbing $Rh_n^{0/\pm}$ (n = 2–8) clusters, *New J. Chem.*, 2018, **42**, 1121–1132.

35 C. Lacaze-Dufaurea, J. Roquesb, C. Mijoulea, E. Siciliac, N. Russoc, V. Alexievd and T. Mineva, A DFT Study of the NO adsorption on Pd_n (n = 1–4) clusters, *J. Mol. Catal. A: Chem.*, 2011, **341**, 28–34.

36 X. Ding, Z. Li, J. Yang, J. G. Hou and Q. Zhu, Theoretical study of nitric oxide adsorption on Au clusters, *J. Chem. Phys.*, 2004, **121**, 2558–2562.

37 Y.-L. Teng, M. Kohyama, M. Haruta and Q. Xu, Infrared spectroscopic and theoretical studies on the formation of Au_2NO^- and Au_nNO (n = 2–5) in solid argon. *J. Chem. Phys.*, 2009, **130**, 134511.

38 S. Hirabayashi and M. Ichihashi, Stability of aluminum-doped copper cluster cations and their reactivity toward NO and O_2, *J. Phys. Chem. A*, 2015, **119**, 8557–8564.

39 S. Hirabayashi and M. Ichihashi, Reactions of Ti- and V-doped Cu cluster cations with nitric oxide and oxygen: size dependence and preferential NO adsorption, *J. Phys. Chem. A*, 2016, **120**, 1637–1643.

40 M. Arakawa, K. Kohara, T. Ito and A. Terasaki, Size-dependent reactivity of aluminum cluster cations toward water molecules, *Eur. Phys. J. D*, 2013, **67**, 80.

41 T. Ito, G. Naresh Patwari, M. Arakawa and A. Terasaki, Water-induced adsorption of carbon monoxide and oxygen on the gold dimer cation, *J. Phys. Chem. A*, 2014, **118**, 8293−8297.

42 M. Arakawa, K. Kohara and A. Terasaki, Reaction of aluminum cluster cations with a mixture of O_2 and H_2O gases: Formation of hydrated-alumina clusters, *J. Phys. Chem. C*, 2015, **119**, 10981−10986.

43 M. Arakawa, T. Omoda and A. Terasaki, Adsorption and subsequent reaction of a water molecule on silicate and silica cluster anions, *J. Phys. Chem. C*, 2017, **121**, 10790−10795.

44 M. Arakawa, K. Ando, S. Fujimoto, S. Mishra, G. Naresh Patwari and A. Terasaki, The role of electronegativity on the extent of nitridation of group 5 metals as revealed by reactions of tantalum cluster cations with ammonia molecules, *Phys. Chem. Chem. Phys.*, 2018, **20**, 13974–13982.

45 T. Ito, M. Arakawa, Y. Taniguchi and A. Terasaki, Adsorption kinetics of nitrogen molecules on size-selected silver cluster cations, *Z. Phys. Chem.*, 2019, **233**, 759–770.

46 M. Arakawa, D. Okada, S. Kono and A. Terasaki, Preadsorption effect of carbon monoxide on reactivity of cobalt cluster cations toward hydrogen, *J. Phys. Chem. A*, 2020, **124**, 9751−9756.

47 S. Sarugaku, M. Arakawa, T. Kawano and A. Terasaki, Electronic and geometric effects on chemical reactivity of 3d-transition-metal-doped silver cluster cations toward oxygen molecules, *J. Phys. Chem. C*, 2019, **123**, 25890−25897.

48 H. Haberland, M. Karrais, M. Mall, Y. Thurner, Thin films from energetic cluster impact: a feasibility study, *J. Vac. Sci. Technol., A*, 1992, **10**, 3266.

49 T. Ito, K. Egashira, K. Tsukiyama and A. Terasaki, Oxidation processes of chromium dimer and trimer cations in an ion trap, *Chem. Phys. Lett.*, 2012, **538**, 19–23.

50 B. C. Guo, K. P. Kerns, A. W. Castleman, Jr., Chemistry and kinetics of size-selected cobalt cluster cations at thermal energies. 2. Reactions with oxygen, *J. Phys. Chem.*, 1992, **96**, 6931–6937.

51 S. Sarugaku, M. Arakawa and A. Terasaki, Space focusing extensively spread ions in time-of-flight mass spectrometry by nonlinear ion acceleration, *Int. J. Mass Spectrom.*, 2017, **414**, 65–69.

52 T. Handa, T. Horio, M. Arakawa and A. Terasaki, Improvement of reflectron time-of-flight mass spectrometer for better convergence of ion beam, *Int. J. Mass Spectrom.*, 2020, **451**, 11631.

53 E. Schumacher, *DETMECH − Chemical Reaction Kinetics Software*, University of Bern, Bern, Switzerland, 2003.

54 V. Zamudio-Bayer, L. Leppert, K. Hirsch, A. Langenberg, J. Rittmann, M. Kossick, M. Vogel, R. Richter, A. Terasaki, T. Möller, B. von Issendorff, S. Kümmel and J. T. Lau, Coordination-driven magnetic-to-nonmagnetic transition in manganese-doped silicon clusters, *Phys. Rev. B*, 2013, **88**, 115425.

55 M. Shibuta, T. Ohta, M. Nakaya, H. Tsunoyama, T. Eguchi and A. Nakajima, Chemical characterization of an alkali-like superatom consisting of a Ta-encapsulating Si_{16} cage, *J. Am. Chem. Soc.*, 2015, **137**, 14015–14018.

56 J. Zhao, Q. Du, S. Zhou and V. Kumar, Endohedrally doped cage clusters, *Chem Rev.*, 2020, **120**, 9021–9163.

57 E. Janssens, S. Neukermans, H. M. T. Nguyen, M. T. Nguyen and P. Lievens, Quenching of the magnetic moment of a transition metal dopant in silver clusters, *Phys. Rev. Lett.*, 2005, **94**, 113401.

58 E. Janssens, S. Neukermans, X. Wang, N. Veldeman, R. E. Silverans and P. Lievens, Stability patterns of transition metal doped silver clusters: Dopant- and size-dependent electron delocalization, *Eur. Phys. J. D*, 2005, **34**, 23–27.

59 R. Dong, X. Chen, H. Zhao, X. Wang, H. Shu, Z. Ding and L. Wei, Structural, electronic and magnetic properties of Ag_nFe clusters ($n \leq 15$): local magnetic moment interacting with delocalized electrons, *J. Phys. B: At., Mol. Opt. Phys.*, 2011, **44**, 035102.

60 V. M. Medel, A. C. Reber, V. Chauhan, P. Sen, A. M. Köster, P. Calaminici and S. N. Khanna, Nature of valence transition and spin moment in Ag_nV^+ clusters, *J. Am. Chem. Soc.*, 2014, **136**, 8229–8236.

61 P. L. Rodríguez-Kessler and A. R. Rodríguez-Domínguez, Structural, electronic, and magnetic properties of Ag_nCo (n = 1–9) clusters: A first-principles study. *Comput. Theor. Chem.*, 2015, 1066, 55−61.

62 P. L. Rodríguez-Kessler, S. Pan, E. Florez, J. L. Cabellos and G. Merino, Structural evolution of the rhodium-doped silver clusters Ag_nRh ($n \leq 15$) and their reactivity toward NO, *J. Phys. Chem. C*, 2017, **121**, 19420−19427.

63 R. Xiong, D. Die, L. Xiao, Y.-G. Xu and X.-Y. Shen, Probing the structural, electronic, and magnetic properties of Ag_nV (n = 1–12) clusters, *Nanoscale Res. Lett.*, 2017, **12**, 625.

64 R. Xiong, D. Die, Y.-G. Xu, B.-X. Zheng and Y.-C. Fu, Probing the structural, electronic and magnetic properties of Ag_nSc (n = 1−16) clusters, *Phys. Chem. Chem. Phys.*, 2018, **20**, 15824−15834.

65 P. Marín, J. A. Alonso, E. Germán and M. J. López, Nanoalloys of metals which do not form bulk alloys: The case of Ag−Co, *J. Phys. Chem. A*, 2020, **124**, 6468−6477.

66 L. Lai, D. Die, B.-X. Zheng and Q. Du, Growth mechanism and electronic and magnetic properties of Ag_nTi alloy clusters, *J. Phys. Chem. Solids*, 2021, **148**, 109757.

67 S. Sarugaku, R. Murakami, J. Matsumoto, T. Kawano, M. Arakawa and A. Terasaki Size-dependent reactivity of nickel-doped silver cluster cations toward oxygen: Electronic and geometric effects, *Chem. Lett.*, 2017, **46**, 385−388.

68 S. Minamikawa, M. Arakawa, K. Tono and A. Terasaki, A Revisit to electronic structures of cobalt-doped silver cluster anions by size-dependent reactivity measurement, *Chem. Phys. Lett.*, 2020, **753**, 137613.